Available online at www.sciencedirect.com

ScienceDirect

Energy Procedia 78 (2015) 1311 – 1316

Energy Procedia

6th International Building Physics Conference, IBPC 2015

Effects of drifting sand particles on deterioration of mural paintings on the east wall of cave 285 in Mogao caves, Dunhuang

Akane Mikayama[a,*], Shuichi Hokoi[a], Daisuke Ogura[a], Ken Okada[b], Bomin Su[c]

[a]*Kyoto University, Kyoto University Katsura, Nishikyo-ku, Kyoto 615-8510, Japan*
[b] *National Research Institute for Cultural Properties, Ueno Park, Taito-ku, Tokyo 110-8713, Japan*
[c]*Dunhuang Academy, Mogao Grottoes, Dunhuang, Gansu 736200 ,China*

Abstract

The Mogao caves, which are designated as a World Heritage site, house the remains of one of the largest collections of Buddhist mural paintings. The cave investigated in this study is cave 285, which has paintings on the walls and ceiling. The purpose of this research is to identify the causes for the deterioration of the paintings, particularly on the east wall. Emphasis is placed on collision and adhesion of sand particles driven by the wind into the cave as a candidate cause of deterioration on the east wall.

Peer-review under responsibility of the CENTRO CONGRESSI INTERNAZIONALE SRL

Keywords: conservation, cultural asset, CFD, sand particle, deterioration

1. Background and purpose of research

The Mogao caves are about 25 km away from the city area of Dunhuang, Gansu Province, China. They were constructed from the 4th through the 14th centuries. There are more than 700 caves consisting of upper, middle, and lower areas, along 2 km distance of Mingsha mountain cliff, with paintings and colored statues remaining in 492 caves. In the surveyed cave 285, the paintings on the walls and ceiling have undergone deterioration in the form of

* Corresponding author. Tel.: +81-75-451-5514; fax: +81-75-451-5514.
E-mail address: be.akane@archi.kyoto-u.ac.jp

Peer-review under responsibility of the CENTRO CONGRESSI INTERNAZIONALE SRL
doi:10.1016/j.egypro.2015.11.146

cracks, detachment, and discoloration. The causes underlying the deterioration have not yet been fully identified. Therefore, it is necessary to clarify the causes for deterioration in order to conserve the paintings in the Mogao caves.

The purpose of this study is to identify the relationship between the deterioration of the paintings on the east wall of cave 285 and the external environment. The entrance hall is known to have collapsed for a certain period in the past. Hence, the cave should have been strongly influenced by the external environment until the new entrance hall was constructed. It is reasonable to assume that flood, underground water, and rain water have little effect on cave 285 because the cave is in the middle layer of a cliff. The influence of solar radiation or natural light may also be minimal on the east wall because cave 285 faces east and its only opening is installed in the east wall. Therefore, collision and adhesion of wind driven sand particles are being investigated as remaining reasons for the deterioration of the east wall. First, we measured the air velocity and direction around the front door to the present entrance hall. Second, we surveyed the particle size distribution of sand. We then simulated the temperature and air-flow distributions in the cave by computational fluid dynamics (CFD) simulations, and compared the spatial distribution of deterioration of the paintings with the air-flow distribution near the east wall. Finally, we simulated the movement of the sand particles.

2. Shape of cave 285 and deterioration status of paintings of east wall

2.1. Floor plan of cave 285

The main room of cave 285 has a nearly square floor plan and a cone-shaped ceiling (Fig. 1, [1]). In the middle of the 20 century, an entrance hall with an east-facing door was constructed on the east side of the main room because the original entrance hall had collapsed at some time in the past. This situation is confirmed by a photograph taken by a Russian expedition team between 1914 and 1915 ([2]). There was no entrance hall at that time, and the opening to the main room directly led to the outside. The present research deals with this period.

2.2. Deterioration of paintings on east wall in cave 285

The following patterns of deterioration are seen in the paintings on the east wall of cave 285 (Fig. 2). (1) Deterioration of the lower part (solid line); this part was once restored from the original paintings. However, there are numerous cracks and detachments on the coloring layer, particularly in the paintings near the opening where they suffer from almost complete loss so that the original state cannot be estimated. The deterioration on the south side is more serious than that on the north side. (2) Deterioration at the upper part of the opening (dotted line); many cracks and detachments can be seen on the paintings on the east wall near the opening. The deterioration on the north side is slightly more serious than that on the south side. (3) Deterioration of the central part of both the north and south sides (broken line); a comparison between the central parts of the north and south sides of the east wall shows more pronounced discoloration, which seem to be caused by adhesion (a state to be stuck to the surface of the paintings), in a wide range and more severe detachment of the base layer on the north side. Adhesion is probably related to the transfer of heat and moisture through a very thin wall between the east wall and a small cave (cave 287), which is adjacent to the outside of the northern east wall (Fig. 1).

3. Wind distribution around Mogao caves and measurement of airflow and temperature distributions at cave 285

3.1. Wind distribution around Mogao caves

A weather station installed by the Dunhuang Academy is located in front of cave 72, which is at a lower cliff height and 200 m south of cave 285. The wind velocity and direction measured at the weather station from January 6, 2011 to December 4, 2013 are shown in Fig. 3. Although the wind direction at the lower cliff height was complicated, there was a tendency for low-speed winds in the northern and northeast directions to be most frequent. Winds in the southeastern direction were much stronger although less frequent. The mean wind velocity over the past three years was approximately 1.1 m/s.

3.2. Measurement of airflow and temperature around cave 285

Near the door to the (present) entrance hall of cave 285, we measured the outside and entrance hall air temperatures along with the prevailing wind velocity and direction at a distance of approximately 1 m from the door. We also recorded the state of 6 streamers placed around the door from 14:00 to 14:30 on September 4, 2013.

The measurement results show that the mean outside and mean entrance hall temperatures were 28.4 °C and 23.8 °C, respectively. The most frequent wind direction during the observation period was north. The airflow distribution around the door is shown in Fig. 4. The distributions of the airflow in the cases of south and north winds were just symmetric, although south winds were less frequent.

4. Particle size distribution of sand collected in cave 285

Several micrographs of the sand particles collected at points (A) to (E) in Fig. 1 are shown in Fig. 5.

The results observed by a microscope show that the deeper the position in the cave, the smaller was the size of the sand particles. The particles seen outside were slightly larger than those seen inside (compare (A) and (B)), and there was little difference between the upper and lower heights ((B) and (C)). The diameter of the largest particle was approximately 0.1 mm and that of the smallest one was less than 0.01 mm at (A), (B), and (C). In contrast, the diameters of the particles in the main room were very narrowly distributed around 0.01 mm.

According to this result, the particle diameter was set to 0.1 mm or 0.01 mm in the following simulations.

5. Simulation of airflow in cave 285

5.1. Simulation in case of northeast wind

The geometry of the simulation model without an entrance room is shown in Fig. 6(a). In the simulation, an outside space of 15.0 m in width, 6.0 m in depth, and 3.0 m in height was assumed on the east side of the cave, as shown in Fig. 6(b). The north end of the outside space was 1 m north of the north end of the opening of the cave.

We performed a one-hour transient calculation with a time increment of 0.25 s by using a high-Reynolds number k-ε turbulence model (STAR-CD, [3]). As the boundary condition of the flow, the entire north surface of the outside space was set as an inlet, and the entire south surface as a pressure-prescribed boundary. The temperature was fixed at the surfaces of the other walls of cave 285 and the outside space. The CFD analysis was performed by assuming a northeastern wind with a mean wind velocity of 1.41 m/s. The most frequent wind (i.e., northeast) was given at the inlet boundary. The following parameter values were used: an incident angle of 45°, a temperature of 28.4 °C obtained by measurement, and a velocity of 1.41 m/s. The temperatures of all wall surfaces were set at 23.8 °C, which was the measured temperature at the entrance hall. The initial temperature was also set at 23.8 °C.

The simulated results of air velocity and direction are shown in Fig. 7(a). The north wind flows into the cave from the upper south side of the opening and flows out from the lower part of the opening. This result at the opening agrees well with the measured result in Fig. 4.

The air velocity distribution in the section at a 5 cm distance from the east wall in the entrance hall is shown in Fig. 7(b). At the lower part of the east wall, the air velocity on the south side (0.09 m/s) is greater than that on the north side (0.05 m/s), although both air velocities are small. At the middle and upper parts of the east wall, there is little difference between the south and north sides, and the air velocity is greater than that in the lower part (over 0.1 m/s).

The relationship between the spatial distributions of airflow and deterioration of the east wall (Figs. 2 and 7(b)) is summarized as follows. (1) Deterioration of the lower part (Fig. 2, solid line); the simulated air velocity near the south side of the east wall is higher than that of the north side. This velocity agrees well with the state of deterioration of the lower part, which is more severe on the south than on the north side. Therefore, it is likely that the collision of wind driven sand is the reason for the deterioration. (2) Deterioration at the upper part of the opening (Fig. 2, dotted line); the air velocity near the north side of the east wall is higher than that near the south side. This also explains the state of deterioration near the opening, which is more severe on the north than on the south side. (3) Deterioration of the central part of both the north and south sides (Fig. 2, broken line); there is little

difference between the air velocities on both sides. However, the discoloring and detachment of the base layer are more severe on the north side. Therefore, another factor may be responsible for this deterioration.

The movement of sand particles was simulated to understand its relation to the airflow ([4], [5]). The particle diameter was set to 0.1 or 0.01 mm based on the particle size distribution obtained in Section 3. One sand particle ([5]) was placed at the upper south side of the opening at the time of 500 s after the CFD calculation was started. The simulated results are shown in Figs. 8(a) and (b). Neither particle flowed into the cave. In the next section, therefore, a simulation was attempted by using a southeast wind with high velocity, considering the wind data measured at the weather station (Fig. 3).

5.2. Simulation in case of southeast wind with greater wind velocity

In this simulation, an outside space with the same size as that in Fig. 6(b) was used, where the south boundary of the outside space was 1 m south of the south end of the opening of the cave as in Fig. 6(c).

We performed a 30-min transient calculation with a time increment of 0.25 s. As the boundary condition of the flow, the south surface of the outside space (except the western most 1 m) was set as the inlet, and the entire north surface as the pressure boundary. The temperature was fixed at the surfaces of all walls of the cave 285 and the outside space. The CFD analysis was performed by assuming a southeastern wind with high velocity. A southeastern wind with an incident angle of 45° and the vertical wind velocity distribution shown in Fig. 9 (with a maximum wind velocity of 4 m/s) was used at the inlet boundary.

The simulated results of air velocity and direction are shown in Fig. 10(a). The result of the simulation agrees well with the measured result in that the southeast wind flows into the cave from the upper north side of the opening and flows out from the lower part of the opening.

The air velocity distribution in the section at a 5 cm distance from the east wall is shown in Fig. 10(b). At the lower part of the east wall, the air velocity on the south side (0.4 m/s) is greater than that on the north side (0.1 m/s). Near the opening, the wind velocity is approximately 0.2 m/s. At the middle and upper parts of the east wall, the wind velocity is small (0.1 m/s), although this is close to the wind velocity in Fig. 7(b).

The relationship between the distributions of airflow and deterioration of the east wall (Figs. 2 and 10(b)) is summarized as follows. (1) Deterioration of lower part; the simulated air velocity corresponds well with the state of deterioration of the lower part, which is more remarkable on the south than on the north side. (2) Deterioration at the upper part of the opening; the wind velocity near the south side of the east wall is higher than that near the north side. This does not agree well with the state of deterioration near the opening, which is more remarkable on the north than on the south side. (3) Deterioration of the central part of both the north and south sides; the air velocity agrees well with the discoloration of the center of the north side.

The same simulation of wind driven particles as that performed in Section 5.4 was carried out. The calculated results are shown in Figs. 8(c) and (d). The particle with a diameter of 0.1 mm flowed into the cave and fell to the floor of the main room. Because the air velocity near the floor was small, it never ascended again. In contrast, the particle with a diameter of 0.01 mm flowed into the cave, moved up and down, and then flowed out through the lower part of the opening.

6. Conclusion

In this research, to clarify the influence of wind driven sand on the deterioration of the paintings on the walls in cave 285 of the Mogao caves in Dunhuang, we measured the distributions of airflow and temperature around the door of the entrance hall, and surveyed the sand particle distribution. We carried out a simulation of airflow assuming a southeast wind with higher velocity based on the weather observation data. The calculated air velocity distribution near the east wall agreed reasonably well with the spatial distribution of deterioration. The particles flowed into the main room. Therefore, sand particles in a southeast wind with high velocity may contribute to the deterioration of the paintings on the east wall.

Acknowledgements

We would like to thank the Dunhuang Academy and National Research Institute for Cultural Properties, Tokyo.

References

[1] Ji Xianlin, Toshio Nagahiro, Chang Shuhong, Duan Wenjie et al. Mogao cave, Dunhuang. Heibonsha Limited, Publishers. 1980
[2] Dunhuang Art Collection offhand. Shanghai Classics Publishing House; 2000.
[3] IDAJ Company, Limited (https://www.idaj.co.jp/). 2013/11/16 access.
[4] Masaru Abuku. Moisture stress of wind-driven rain on building enclosures. PROCOPIA; 2009.
[5] Aytaç Kubilay. Numerical (CFD) simulations and field experiments of wetting of building facades due to wind-driven rain in urban areas. Doctor thesis; 2014.

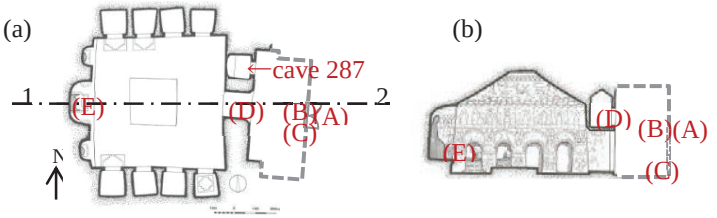

Fig. 1 Outlines of cave 285: (a) floor plan; (b) east-west section (section 1-2).

Fig. 2 East wall of cave 285.

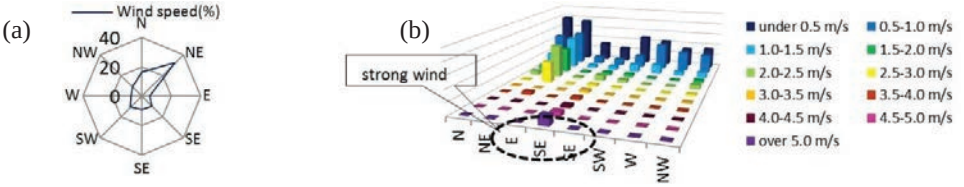

Fig. 3. Wind distribution at weather station: (a) wind rose; (b) frequency of wind direction and velocity.

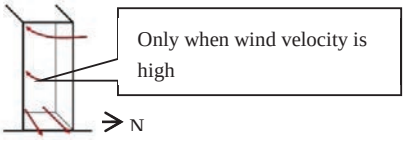

Fig. 4. Airflow around door when north wind blows.

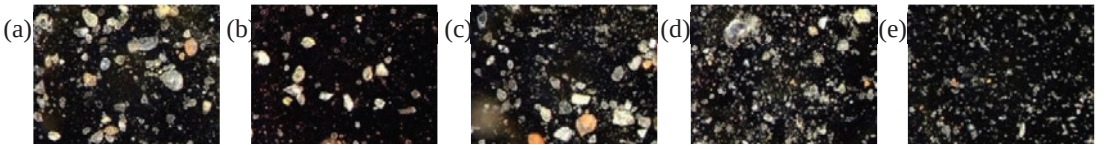

Fig. 5. Micrographs of sand: (a) at point (A); (b) at point (B); (c) at point (C); (d) at point (D); (e) at point (E).

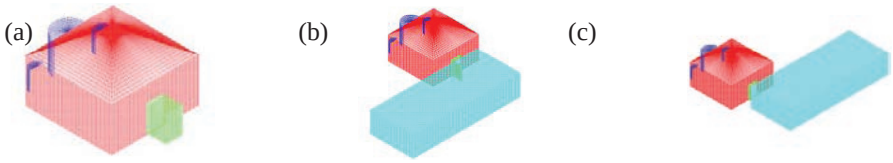

Fig. 6. Simulation models: (a) model without entrance hall; (b) model used in Section 5; (c) model used in Section 6.

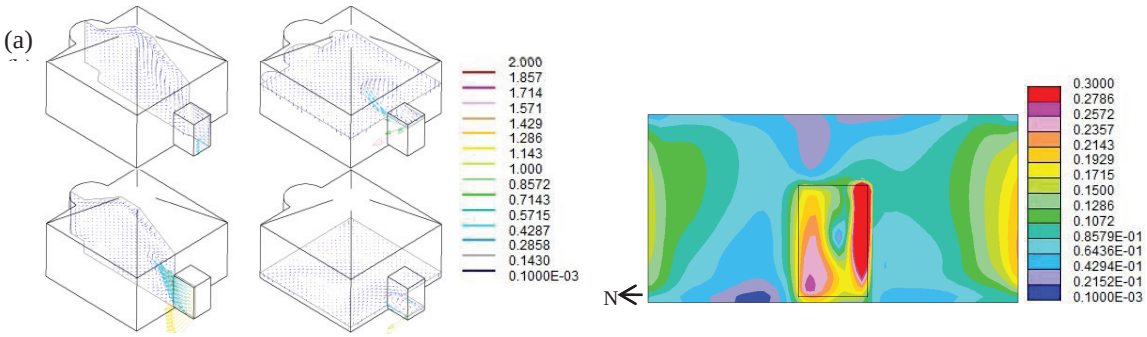

Fig. 7 Air velocity and direction: (a) airflow distribution in cave 285; (b) wind velocity distribution near east wall (viewed from inside).

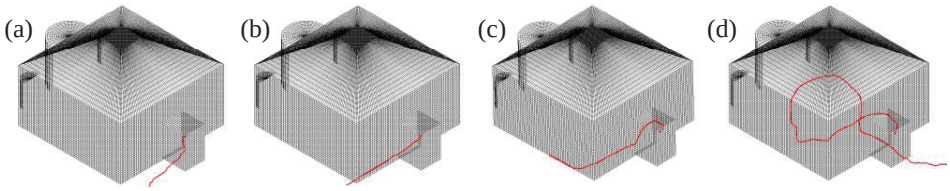

Fig. 8 Movement of particles: (a) trajectory of particle with diameter of 0.1 mm; (b) trajectory of the particle with diameter of 0.01 mm; (c) trajectory of particle with diameter of 0.1 mm; (d) trajectory of particle with diameter of 0.01 mm.

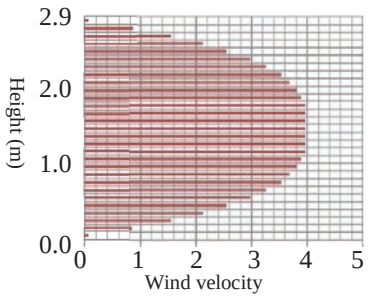

Fig. 9 Vertical wind velocity distribution at inlet boundary

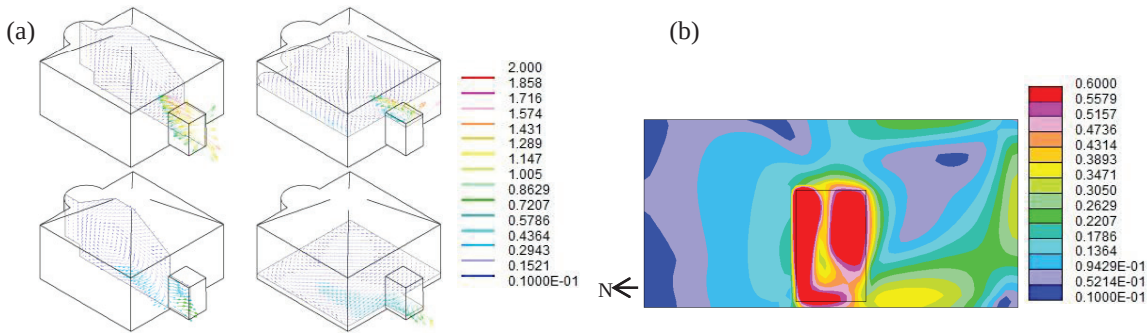

Fig. 10 Air velocity and direction: (a) airflow distribution in cave 285; (b) wind velocity distribution near east wall (viewed from inside).